J Mater Sci (2019) 54:3805–3816

Chemical routes to materials

Synthesis of nitrogen-rich hollow microspheres for CO_2 adsorption

Fengqin Yin[1], Zhejia Wu[1], Xianyong Luo[1], Linzhou Zhuang[1,3], Haozhen Ou[1], and Shuixia Chen[1,2,*]

[1] PCFM Lab, School of Chemistry, Sun Yat-Sen University, Guangzhou 510275, People's Republic of China
[2] Materials Science Institute, Sun Yat-Sen University, Guangzhou 510275, People's Republic of China
[3] School of Chemical Engineering, University of Queensland, St Lucia, QLD 4072, Australia

Received: 29 August 2018
Accepted: 1 November 2018
Published online: 12 November 2018

ABSTRACT

The nitrogen-rich hollow microspheres (MFM) with different pore sizes have been synthesized by using melamine, *m*-phenylenediamine and paraformaldehyde as monomer, different particle sizes of SiO_2 microsphere as template, and water as solvent. The specific surface area, pore volume and average pore size of the synthesized MFM were 183.67 m^2/g, 0.91 cm^3/g and 19.8 nm, respectively. After loading polyethyleneimine (PEI), its CO_2 adsorption capacity could reach 2.68 mmol/g at 60 °C, with the corresponding utilization efficiency of amino as high as 40.66%. The kinetic simulation of pseudo-first-order, pseudo-second-order and Avrami kinetic model showed that the Avrami model could better describe the adsorption process of CO_2, indicating both physical adsorption and chemical adsorption in the whole process. The diffusion mechanism was simulated by using the Boyd model, the intermolecular diffusion model and the intraparticle diffusion model, showing that the porous structure of MFM was beneficial to the diffusion of CO_2 in the particles. After 5 cycles, 10 cycles, 15 cycles and even after 20 cycles of adsorption–desorption, the adsorption capacity of MFM-PEI at 30 °C was nearly the same as the capacity of the fresh one, indicating the regeneration stability of the adsorbent, with great advantages in practical production.

Introduction

In recent years, the enormous amount of CO_2 emitted from fossil fuel has become a problem that receives increasing attention and urgently needs to be solved since it has resulted in greenhouse effect as well as another series of environmental problems [1–5]. To reduce the emission of CO_2, carbon capture and storage (CCS) is considered as a satisfactory approach, where the solid amine adsorption material that is developed with the adsorption method as the core is one of the most effective adsorption materials [6–10]. Currently, the solid amine adsorbent is commonly synthesized by employing porous materials as

Address correspondence to E-mail: cescsx@mail.sysu.edu.cn

https://doi.org/10.1007/s10853-018-3107-5

matrix and following by introducing amine reagents via physical or chemical method [11, 12]. However, the existing porous polymer materials are rather rigid and unable to carry out post-processing and secondary molding treatment, which greatly limits its application in practice [13, 14]. In addition, most of the porous matrices were synthesized in the form of powder and need to use a lot of organic solvents in the prepared process. When running CO_2 capture, it is easy to cause the blockage of adsorption column, leading to poor dynamic performance [15–18].

In general, the adsorption capability of solid amine adsorbent largely depends on specific surface area of the matrix and its porosity, pore volume, constituent elements and so on [19–21]. According to the previous report, high nitrogen content in a way facilitates the adsorption performance of porous materials, especially in the selective adsorption [22–26]. And there is a new concept called N_2 phobicity. Wang et al. [27] prepared porous polymers with surface area and nitrogen content of 744 m^2/g and 10.21% using 1, 4-phthalaldehyde and benzene as monomers and DMSO as solvent. After carbonization, its nitrogen content reached 5.58–8.74% and showed good CO_2 adsorption and selective adsorption performance. Under the conditions of 1 bar and room temperature, its adsorption capacity of CO_2 was 7.41 μmol, which was the best value of porous carbon material for CO_2 adsorption at that time. Lee et al. [28] used melamine and phenol as monomer and F127 as template to synthesize a highly ordered mesoporous polymer, whose nitrogen content was as high as 18%. Since it was rich in nitrogen and with great pore size distribution (2.5–2.9 nm), it showed favorable CO_2 selectivity that increased with temperature and reached its maximum of 117 (Henry method) at 323 K.

According to the above, it can be seen that the nitrogen-rich porous material has good adsorption and selective adsorption to CO_2 [28–32]. Among the many nitrogen-rich monomers, melamine has the advantages of weak basicity (pKa = 5.5), diverse reactivity, high nitrogen content, inexpensive and extensive sources, which promotes the relevant research and application as well as attracts widespread attention of scientific research workers [19, 20, 33]. It also has been reported that the absorbent, prepared by melamine immobilized on the surface of porous silicon or melamine combined into the covalent organic framework (COF) structure, showed better adsorption performance for CO_2 [34]. In this paper, a series of MFM with different pore diameters were synthesized in water solvent by using melamine, formaldehyde and *m*-phenylenediamine as monomers and SiO_2 microspheres with different particle diameters as templates. These hollow microspheres were used as the matrix to load PEI and prepared solid amine adsorbents with different pore sizes, whose influence on CO_2 adsorption performance was studied.

Experimental

Reagents

Melamine (AR), poly (ethylenimine) (PEI, *Mw* = 600) and metaphenylene diamine were from Aladdin Chemistry Co., Ltd., China. Formaldehyde aqueous solution (CH_2OH, 37 wt%) and ethyl alcohol were purchased from Guangzhou Chemical Reagent Factory, China. All reagents were used without further purification.

Synthesis of nitrogen-rich hollow microspheres (MFM)

In a typical preparation process, melamine (1.15 g, 9.13 mmol) and formaldehyde aqueous solution (2.23 g, 27.5 mmol) were dissolved in 20 mL water, and then, the mixture was stirred at 90 °C until it became transparent to prepare their prepolymer. The SiO_2 microspheres with different particle sizes (12 nm, 20 nm, 30 nm, 50 nm) and 20 ml metaphenylene diamine aqueous solution were then added into the above prepolymer solution of melamine and formaldehyde. The mixture solution was then carefully transferred to a Teflon container and heated at 120 °C for 5 h to complete the polycondensation of prepolymer (melamine and formaldehyde aqueous solution) and metaphenylene diamine. The polycondensation product, a yellow solid, was ground, sieved and then successively washed with ethyl alcohol. The obtained granules were dried under vacuum at 80 °C and noted as MFM-SiO_2-Xnm, where *X* presents the particle size of SiO_2 microspheres. The formation mechanism is shown in Scheme 1.

Preparation of PEI impregnation sorbents (MFM-PEI)

The nitrogen-rich hollow microspheres (MFM) was modified by impregnating PEI. In a typical process, 0.5 g PEI was dissolved in 20 mL ethanol, and then, 0.5 g MFM was added into the solution. The mixture was continuously stirred at 70 °C for 5 h. After being centrifuged with 10000 r/min for 20 min, the adsorbent was obtained and was dried under vacuum at 80 °C. The resulting adsorbents were denoted as MFM-PEI.

Characterization

Nitrogen adsorption–desorption isotherms were characterized at 77 K on an automatic gas adsorption instrument (ASAP2020, Micromeritics Corp., USA) at the range of relative pressure from 10^{-6} to 1. Before each test, the sample was dried under vacuum at 100 °C overnight. V_{total} was calculated based on the nitrogen amount adsorbed at $P/P_0 = 0.95$. Specific surface area and pore parameters were calculated by using the Brunauer–Emmett–Teller (BET) method and density functional theory (DFT) method, respectively. Scanning electron microscope (SEM, S4800, Hitachi, Japan) was used to observe the morphology and microstructure of the samples, and transmission electron microscope (TEM, JEM-2010HR, JEOL, Japan) was applied to observe the porous structure. ^{13}C solid-state nuclear magnetic resonance (^{13}C NMR) was performed on Mercury-Plus 300 spectrometer (Varian Co., Ltd., American) operating at 400 MHz, and the chemical shifts are quoted relative to the metaphenylene diamine and the polymer.

Scheme 1 Formation mechanism of MFM.

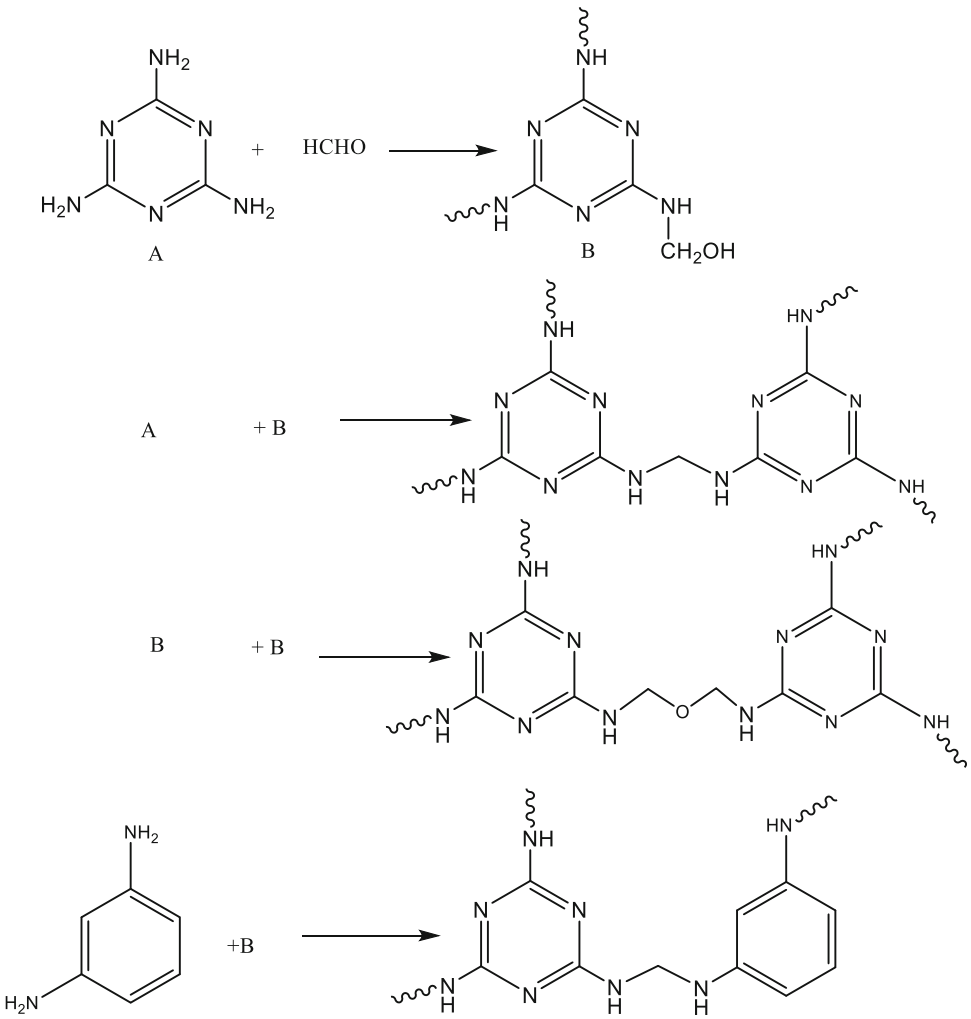

The CO_2 adsorption measurement

The CO_2 adsorption capacity was measured in a fixed bed flow system. Before measurement, the sample was dried under vacuum at 80 °C for 12 h. Then, 0.5 g dried adsorbent was loaded into a glass tube (Φ = 1.3 cm). The dry nitrogen with a flow rate of 30 mL/min was introduced into the column at 90 °C for 20 min to remove the air and residue water. Then, the column was cooled down to room temperature. A mixed gas that includes 10% CO_2 and 90% N_2 with a flow rate of 30 mL/min was introduced to the tube for the adsorption test. The CO_2 concentrations at the inlet and outlet were determined by an Agilent 6820 gas chromatography that is equipped with a thermal conductivity detector. After completing CO_2 adsorption, the adsorbent was regenerated by purging with N_2 with a flow rate of 30 ml/min at 90 °C.

The adsorption capacity was calculated by the following equation:

$$Q = \int_0^t (C_{in} - C_{eff}) \cdot V \cdot dt/22.4W \quad (1)$$

where Q is the adsorption capacity of the adsorbent (mmol CO_2/g); t is the adsorption time (min); C_{in} and C_{eff} are the influent and effluent concentrations of CO_2 (vol%), respectively; V is the total flow rate, 30 mL/min; and W and 22.4 are the weight of the adsorbent (g) and molar volume of gas (mL/mmol), respectively.

Results and discussion

Chemical characterization and pore structure of MFM

MFM with different pore sizes have been successfully synthesized via precipitation polymerization of melamine, formaldehyde solution and metaphenylene diamine in aqueous solution by using different particle size SiO_2 microspheres as template, followed by NaOH extraction. To confirm the chemical structure, solid-state ^{13}C NMR was measured and is shown in Fig. 1. The signals at 165 ppm are indicative of triazine rings. The signal at 68 ppm is associated with the methylene groups in ether linkages, whereas the 53 ppm resonance is attributed to methylene linkages. Moreover, the benzene ring adsorption peak appears in 124 ppm and 150 ppm. The ^{13}C NMR results confirm that the metaphenylene has reacted with methylated melamine and formed methylene groups by dewatering. In addition, according to the analysis of element of the material (Table 1), the nitrogen content of MFM reaches up to 38.52%.

The N_2 adsorption–desorption isotherms of MFMs which were prepared by using different particle size SiO_2 templates are shown in Fig. 2. As illustrated in Fig. 2, the N_2 adsorption–desorption isotherms of MFMs are consistent with type IV isotherm and both of them have hysteresis loops, which indicates that MFMs are mesoporous. The pore structure parameters of MFM hollow microspheres prepared by using different particle size SiO_2 microspheres as templates are presented in Table 2. From Table 2, it can be seen that the specific surface area, pore volume and average pore size of MFM decreased with the increase in SiO_2 particle size. When the particle size of SiO_2 was 12 nm, the MFM hollow microsphere presents the maximum specific surface area, pore volume and average pore size, and their values are 183.67 m^2/g, 0.91 cm^3/g and 19.8 nm, respectively. In the case of the addition of same volume of SiO_2 emulsion, the smaller the particle size of the SiO_2 template, the larger the specific surface area of the MFM hollow microspheres. When the particle size of the template increased, it was difficult for the prepolymer to wrap the template, which resulted in the decrease in the specific surface area, pore volume and average pore size of MFM hollow microspheres.

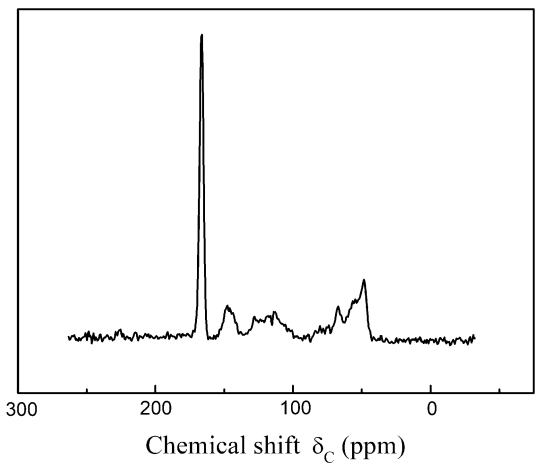

Figure 1 Solid-state ^{13}C NMR spectra of MFM.

Table 1 Element analysis of MFM

Sample	C (%)	N (%)	H (%)	C/N
MFM	44.51	38.52	5.46	1.16

SEM and TEM images of MFM hollow microspheres prepared by using different particle size SiO_2 microspheres as template are shown in Fig. 3. As shown in Fig. 3a, the microspheres show regular spherical morphology, good dispersion and uniform particle size. It can be observed from the TEM image that the MFM microspheres have no pore before the removal of the SiO_2 template (Fig. 3b). The MFM microsphere showed hollow structure after the removal of the SiO_2 template by NaOH dissolving (Fig. 3c–f). The pore sizes of MFM were getting larger as the size of SiO_2 microspheres increased, which is different with the tendency of overall average pore size, implying that the pores in MFM originated not only from the SiO_2 template, but also from the stacking of the polymer particles.

The CO_2 adsorption performance of MFM impregnating PEI (MFM-PEI)

The MFM prepared by using different particle sizes of SiO_2 microspheres as template was used as support to load PEI for CO_2 adsorption. With the increase in particle size of SiO_2 template, the CO_2

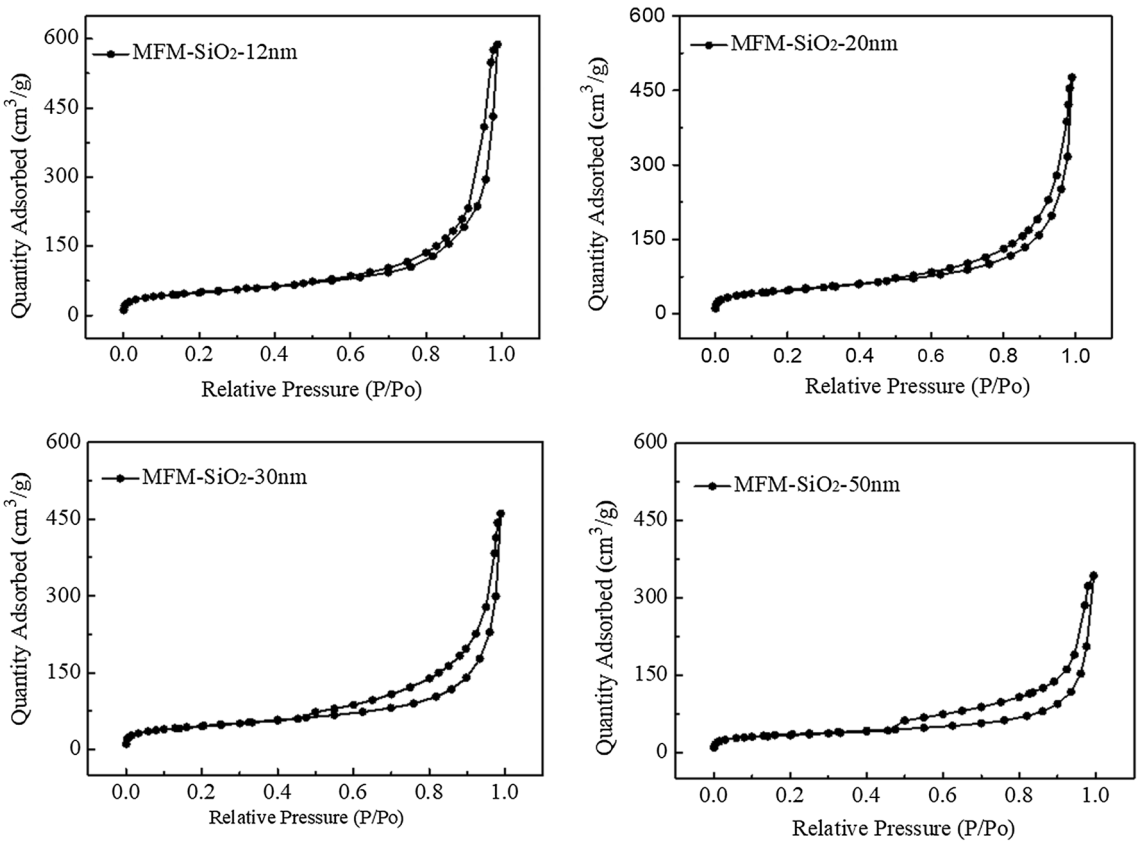

Figure 2 N_2 adsorption–desorption isotherms of MFM-SiO_2 prepared by using different particle sizes of SiO_2 microspheres as template.

Table 2 Pore structure parameter of MFM-SiO_2 prepared by using different particle sizes of SiO_2 microspheres as template

Sample	BET specific surface area (m^2/g)	Pore volume (cm^3/g)	Average pore width (nm)
MFM-SiO_2-12 nm	183.67	0.91	19.80
MFM-SiO_2-20 nm	175.26	0.74	16.81
MFM-SiO_2-30 nm	167.59	0.71	17.02
MFM-SiO_2-50 nm	128.13	0.53	16.55

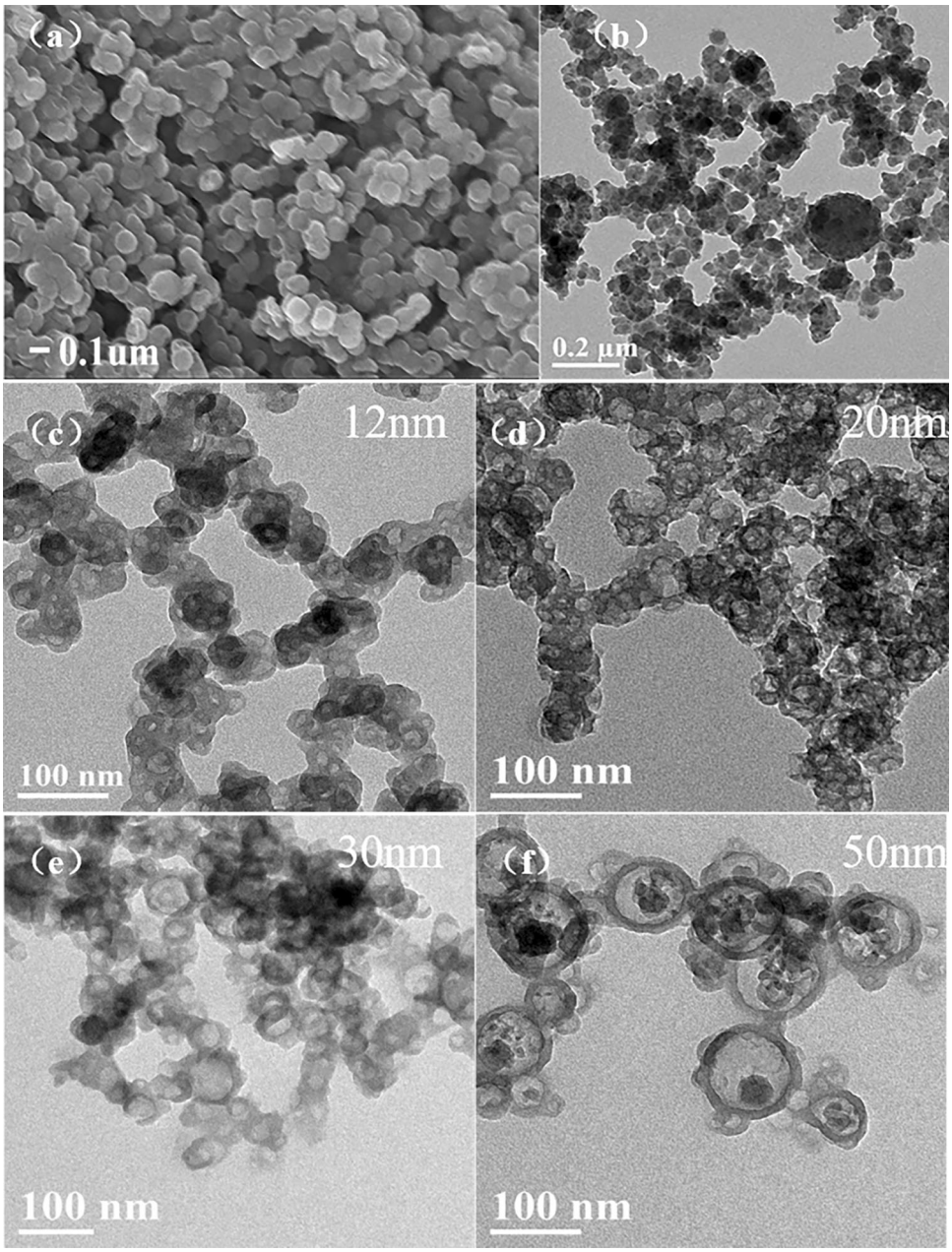

Figure 3 SEM (**a**) and TEM (**b**) images of MFM before the removal of SiO_2 template. The TEM (**c**–**f**) images of MFM after the removal of different particle size SiO_2 templates (12, 20, 30 and 50 nm).

adsorption capacity of MFM-PEI decreases gradually (Fig. 4), which was positively correlated with the specific surface area of MFM, indicating that high specific surface area can increase the contact probability between PEI and CO_2, thus increasing the CO_2 adsorption.

The effect of template dosage on the CO_2 adsorption performance is shown in Fig. 5. It is evident that the dosage of 12 nm SiO_2 microspheres could affect the CO_2 adsorption capacity of MFM-PEI. The adsorption capacity of MFM-PEI increased first and then decreased with the increased dosage of 12 nm SiO_2 microspheres. When the dosage of SiO_2 microspheres was 0.5 mL, the adsorption capacity of MFM-PEI was the largest. Because the pore formation of SiO_2 microspheres was weak when the dosage of SiO_2 microspheres was less, MFM had lower pore volume; accordingly, the loading amount of PEI was lower, leading to lower CO_2 adsorption capacity. With the increase in the dosage of 12 nm SiO_2 microspheres, the specific surface area of MFM increased, but the material became tightness (Fig. 6) and was not beneficial to the diffusion of CO_2, which

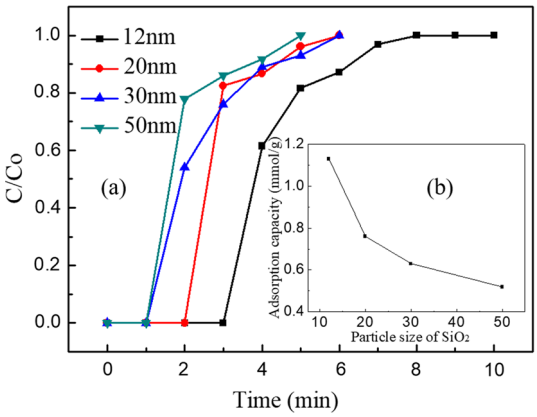

Figure 4 Breakthrough curves (**a**) and capacity (**b**) of CO_2 adsorption on MFM-PEI prepared by using different particle size SiO_2 templates.

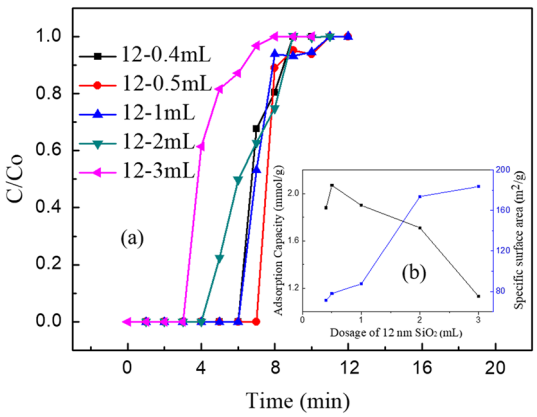

Figure 5 Breakthrough curves (**a**), capacity of CO_2 adsorption on MFM-PEI and specific surface area of MFM (**b**) prepared by using different dosages of 12 nm SiO_2 microspheres.

would also lead to the decrease in CO_2 adsorption capacity.

On the other hand, the CO_2 adsorption capacity of MFM-PEI is largely dependent on the adsorption temperature as indicated in Fig. 7. When the adsorption temperature increased from 20 to 70 °C, the CO_2 adsorption capacity of MFM-SiO_2-12 nm-PEI increased first and then decreased, and the maximum adsorption capacity was 2.68 mmol/g with the corresponding utilization efficiency of amino as high as 40.66% at 60 °C. There are two aspects of the influence of temperature on the adsorption of CO_2 [35, 36]. On the one hand, the adsorption process was controlled by diffusion at low temperatures. The increase in temperature would accelerate the diffusion of CO_2 in thick layer of PEI, and meanwhile, it was beneficial to the complete extension of PEI chains. It exposed the entrapped amino and thus provided more adsorption sites, making it fully contact with CO_2 and improving the CO_2 adsorption capacity with the increase in temperature. On the other hand, the amino group on CO_2 adsorption was exothermic process. The higher temperature made the reaction tend to proceed in the reverse direction, and desorption became the main process under high temperature. Taking these two aspects into account, the adsorption capacity of the material increased first and then decreased with the increase in temperature and had the maximum adsorption capacity at 60 °C.

The regeneration performance of the solid amino sorbents is another significant parameter, as the adsorbent should remain stable CO_2 adsorption capacity for long-term adsorption–desorption cycling in practical application. In Fig. 8, the regenerability of the MFM adsorbents is demonstrated in 20 cycles. After 20 cycles of adsorption (at 30 °C)–desorption (at 90 °C), the MFM-SiO_2-12 nm-PEI adsorbent has no significant decrease in CO_2 adsorption capacity and nearly maintain the same capacity as the fresh one. This result implied that the MFM-SiO_2-12 nm-PEI adsorbents could keep stable for long-term adsorption–desorption cycling.

Primary exploration of adsorption mechanism

In order to better understand the adsorption behavior and adsorption kinetics, the fitting curves of pseudo-first-order models, pseudo-second-order model and Avrami model were drawn to analyze the kinetic mechanism. The fitting parameters with coefficient of determination (R_2) are presented in Table 2. The equations can be arranged as:

$$\text{Lagergren pseudo-first-order: } q_t = q_e\left(1 - e^{k_f t}\right) \quad (2)$$

$$\text{Pseudo-second-order: } q_t = q_e(q_e k_s/(1 + q_e k_s t)) \quad (3)$$

$$\text{Avrami: } q_t = q_e[1 - \exp(-(k_a t)^n)] \quad (4)$$

where t is the time elapsed from the beginning of the adsorption process, q_t is the amount adsorbed at a given point in time and q_e represents the amount adsorbed at equilibrium. k_f (min^{-1}), k_s (g $mmol^{-1}$ - min^{-1}) and k_a (min^{-1}) are rate constants, respectively.

Figure 9 shows the CO_2 adsorption amount of microspheres under different temperatures. The fitting results attained with coefficient of determination (R^2) are listed in Table 3. It can be observed from

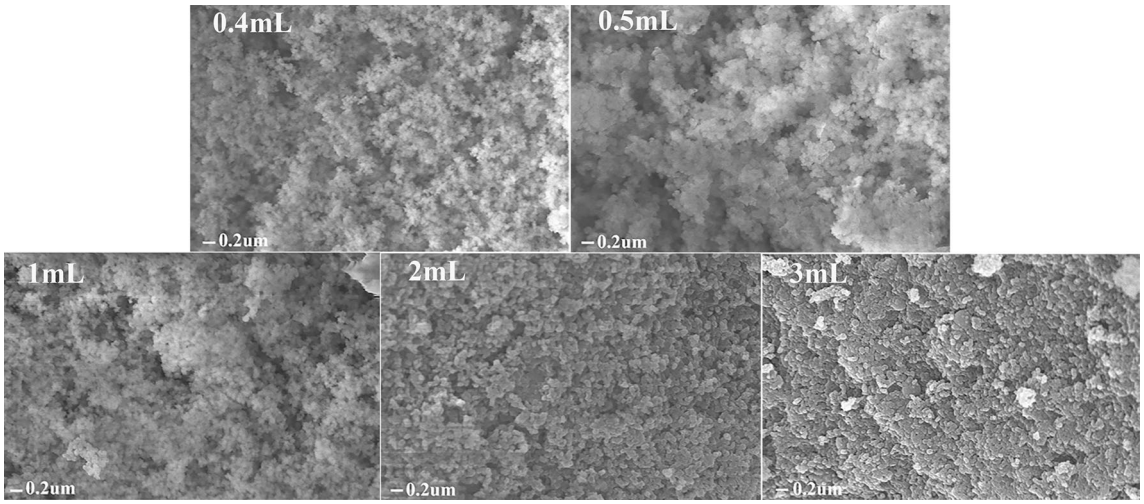

Figure 6 SEM images of MFM prepared by using different dosages 12 nm SiO_2 microspheres.

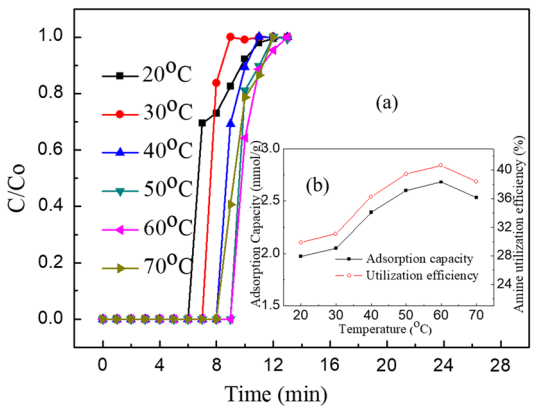

Figure 7 Breakthrough curve (**a**), capacity and amine utilization efficiency (**b**) of CO_2 adsorption on MFM-SiO_2-12 nm-PEI at different temperatures.

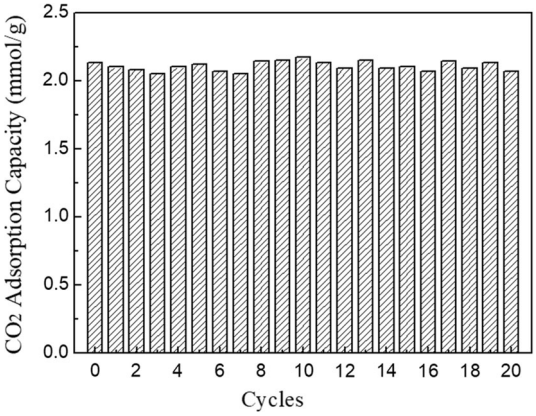

Figure 8 Adsorption capacity of CO_2 on fresh and regenerated MFM-SiO_2-12 nm-PEI.

Fig. 9 that the plots of pseudo-first-order models and pseudo-second-order model failed to match the experimental data as they overrated the CO_2 adsorption at the initial stage and underrated it afterwards. In contrast, the Avrami model fits them well, which was confirmed by the significantly high R^2 (> 0.99), and the forecasts of equilibrium adsorption (q_e) were more approximate to experimental value. Thus, the Avrami model was selected in further analysis of CO_2 adsorption behaviors.

As shown in Fig. 9, the plots can be divided into two stages: At the first stage, the CO_2 was adsorbed completely, leading to a rapidly rising of adsorption amount through time, while at the latter stage, the CO_2 partly breakthrough the adsorbent and the adsorption amount increased slowly before

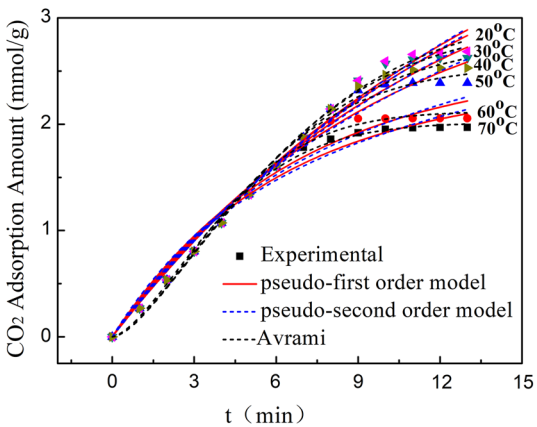

Figure 9 Experimental CO_2 capacity on MFM-SiO_2-12 nm-PEI under different temperatures and corresponding fit to kinetic models.

Table 3 Kinetic parameters for CO_2 adsorption on MFM-SiO_2-12 nm-PEI under different temperatures

Kinetic model	Parameter	Temperature (°C)					
		20	30	40	50	60	70
Pseudo-first-order model	q_e (Exp)	1.970	2.055	2.388	2.624	2.683	2.530
	q_e (Fit)	2.372	2.563	3.509	4.642	5.016	4.090
	K_f	0.166	0.154	0.103	0.073	0.066	0.084
	R^2	0.978	0.969	0.978	0.984	0.987	0.984
Pseudo-second-order model	q_e	3.492	3.848	5.708	7.983	8.735	6.869
	K_s	0.0348	0.0284	0.0114	0.0054	0.0044	0.0075
	R^2	0.970	0.962	0.975	0.983	0.985	0.982
Avrami	q_e	2.015	2.119	2.547	2.947	3.0727	2.773
	Ka	0.0984	0.0821	0.0691	0.0623	0.0614	0.0666
	n	1.534	1.617	1.532	1.456	1.426	1.470
	R^2	0.996	0.992	0.993	0.993	0.994	0.994

equilibrium. As listed in Table 3, the kinetic orders (n_a) varied from 1.4 to 1.7, which means both chemisorption and physisorption play roles in the adsorption of CO_2. And the rate constant (k_a) decreased with temperature at low temperatures but then increased as the temperature exceeding 60 °C, which is consistent with the analysis of Fig. 9.

Whereas the pseudo-first-order models, pseudo-second-order model and Avrami model are only concerned with the CO_2 adsorption process, the Boyd's film-diffusion model, interparticle diffusion model and intraparticle diffusion model were utilized to analyze the experimental kinetic to further insight the rate-controlling step and diffusion rate.

The Boyd's film-diffusion model is expressed as:

$$B_t = \left(\sqrt{\pi} - \sqrt{\pi - \frac{\pi^2 F}{3}}\right)^2 (F < 0.85) \tag{5}$$

$$B_t = -0.4977 - \ln(1 - F)(F > 0.85) \tag{6}$$

$$F = \frac{q_t}{q_e} \tag{7}$$

The interparticle diffusion model is expressed as:

$$q_t = q_e - q_e \frac{6}{\pi^2} e^{\frac{-\pi^2 k_f t}{15}} \tag{8}$$

The intraparticle diffusion model is expressed as:

$$q_t = k_{id} t^{1/2} + C \tag{9}$$

where q_e (mmol g^{-1}) and q_t (mmol g^{-1}) refer to the amount of CO_2 adsorbed at equilibrium and at a given point of time t (min), respectively; C represents the boundary layer thickness; k_f (mmol g^{-1}) and k_{id} (mmol g^{-1}) refer to the interparticle diffusion and intraparticle diffusion rate constant, respectively; F is the fractional attainment of equilibrium at a given point of time; and B_t is a mathematical function of F.

Figure 10 displays the plots of Boyd's film diffusion for B_t against time. According to the Boyd's film-diffusion theory, the nonlinear plots indicated that the CO_2 adsorption behavior of microspheres involves not only film diffusion but also the pore diffusion and chemical reactions. Figure 11 shows the CO_2 adsorption amount of microspheres at the temperature ranging from 20 to 70 °C with plots of interparticle diffusion models drawn on it, and the results attained are listed in Table 4. As shown in Fig. 11, the plots shifted from experimental data with time. And the corresponding R^2 was relatively low, while the predictive q_e was overrated.

To better analyze the diffusion behavior of CO_2 adsorption of microspheres, the intraparticle diffusion model [35, 37] was used. Figure 12 shows the

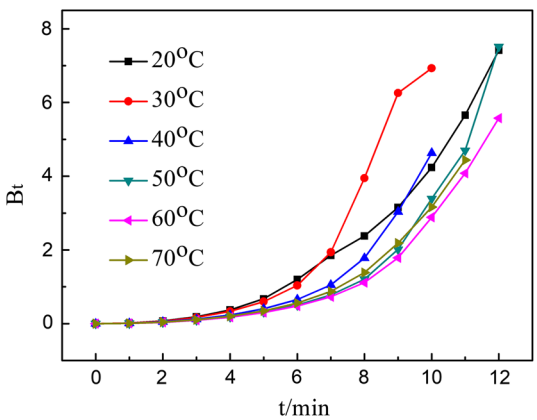

Figure 10 Boyd's film-diffusion simulation curves of MFM-SiO_2-12 nm-PEI under different temperatures.

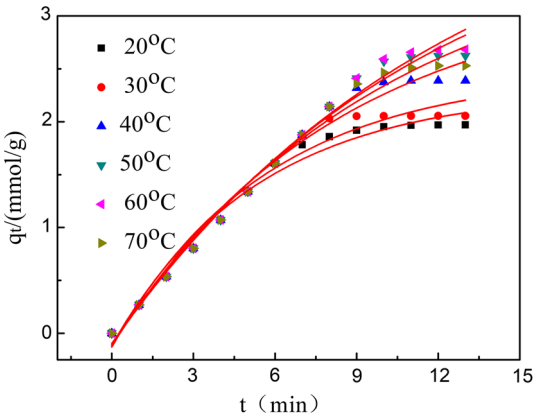

Figure 11 Interparticle diffusion simulation curves of MFM-SiO_2-12 nm-PEI under different temperatures.

Table 4 Parameters of interparticle diffusion simulation of MFM-SiO_2-12 nm-PEI under different temperatures

T (°C)	Parameters				Q (mmol/g)
	q_e (mmol/g)	k_f	R^2	Err/qe	
20	2.300	0.283	0.980	5.465	1.970
30	2.469	0.267	0.971	7.221	2.055
40	3.282	0.183	0.980	10.367	2.388
50	4.211	0.132	0.985	13.972	2.624
60	4.515	0.121	0.987	14.639	2.683
70	3.768	0.152	0.985	11.552	2.530

Weber–Morris plots (the plots of intraparticle diffusion model), which can be divided into three parts that are corresponding to three stages of diffusion. At the first stage, which was the initial stage of adsorption, the CO_2 was outside the particles where the film diffusion controlled the adsorption rate. At the second stage, the medium stage of adsorption, the CO_2 penetrated through the interface layer into the particles, where pore diffusion controlled the adsorption. At the last stage, the CO_2 was inside the pores of particles; thus, the surface reaction dominates the adsorption rate. Figure 12 illustrates that at the 40 °C, the slopes of three parts of plots were 0.27, 1.157 and 2.286. The first stage had the lowest slope, demonstrating the film diffusion controlled the adsorption rate. However, as for the other temperature, the last stages owned the lowest slope, indicating the surface reaction controlled the adsorption rate. Taking 30 °C for an example, the slopes were 0.27, 1.09 and 0.024. And for all of the temperatures considered, the slopes of second stages were always the highest, suggesting that pore diffusion of CO_2 was rather efficient.

The mass transfer rate in MFM-PEI microspheres prepared in this study was compared with that of similar mesoporous amino resin powder adsorbents (MF powder). The time taken to adsorb 1 mmol of CO_2 per unit volume of powder adsorbent and

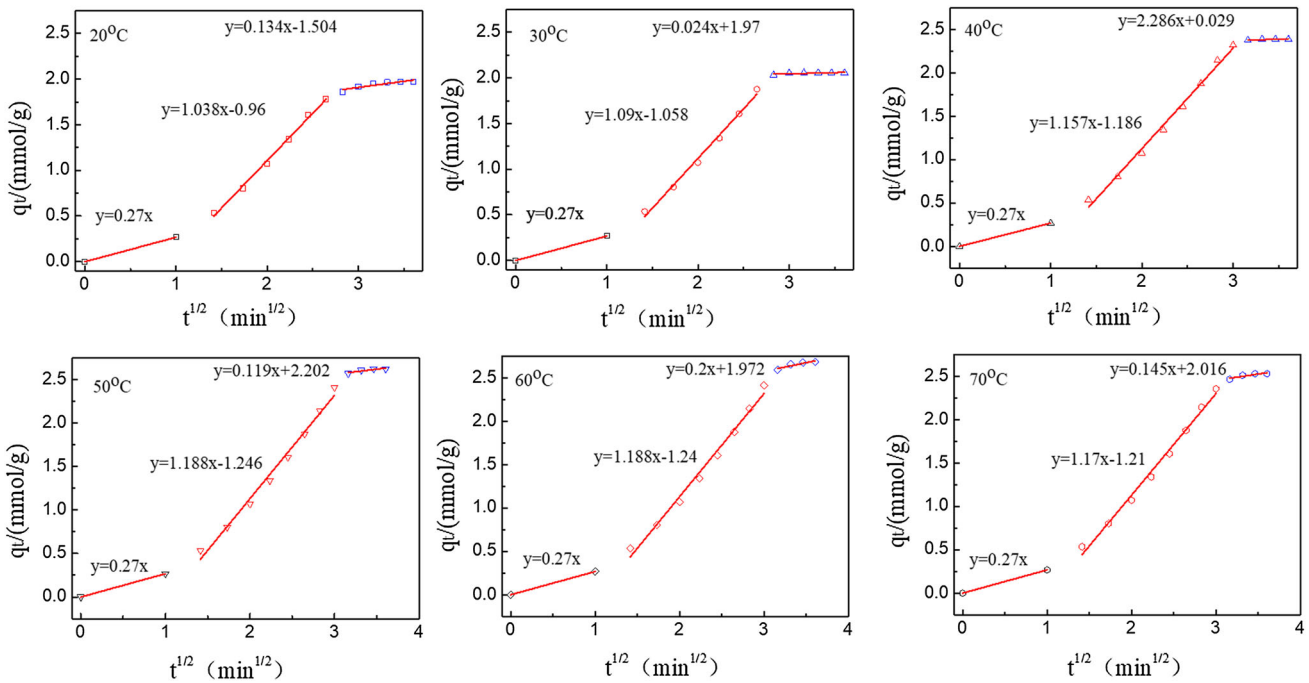

Figure 12 Intraparticle diffusion simulation curves of MFM-SiO_2-12 nm-PEI under different temperatures.

Table 5 Adsorption time used for 1 mmol CO_2 of mesoporous amino resin powder (MF powder) and MFM

Temperature (°C)	Sample	20	30	40	50	60	70
t_{eq} (min)	MF powder	14	16	18	15	15	12
	MFM	10	8	10	11	13	11
Q (mmol/g)	MF powder	3.00	3.77	4.68	3.78	3.22	2.28
	MFM	1.95	2.03	2.37	2.61	2.68	2.51
t (min/mmol.ml)	MF powder	1.02	0.92	0.84	0.86	1.01	0.93
	MFM	0.73	0.56	0.6	0.6	0.6	0.6

microsphere adsorbent was calculated. For this calculation, 0.5 g mesoporous amino resin powder (4.6 ml in volume) and 0.5 g microspheres (7 ml in volume) were separately packed in two glass tubes with the same diameter. The equilibrium adsorption time t_{eq}, the amount of CO_2 adsorbed at equilibrium Q, and the time that taken to adsorb 1 mmol of CO_2 per unit volume of powder or microspheres t were measured.

It could be seen from Table 5 that the time required for MFM to adsorb 1 mmol CO_2 was obviously shorter than that required for the powder mesoporous amino resin, which indicated that the mass transfer rate of gas was obviously increased by the MFM.

Conclusion

In summary, we have successfully prepared the MFM with different pore sizes via precipitation polymerization of melamine, formaldehyde solution and metaphenylene diamine in aqueous solution by using different particle size SiO_2 microspheres as template. When 12 nm SiO_2 microspheres was used as template, the prepared MFM had relatively high specific surface area, pore volume and pore size, which were 183.67 m^2/g, 0.91 cm^3/g and 19.8 nm, respectively. After loading with PEI, the CO_2 adsorption capacity of MFM-PEI reached 2.68 mmol/g at 60 °C, with the corresponding utilization efficiency of amino as high as 40.66%. Avrami model could better describe the adsorption process of CO_2, indicating both physical adsorption and chemical adsorption in the whole process. After 5 times, 10 times, 15 times and even after 20 cycles of adsorption (30 °C)–desorption (90 °C), the adsorption capacity of regenerated MFM-PEI at 30 °C was nearly the same as the that of fresh one, which showed that the adsorbent regeneration performance was stable, and showed higher quick mass transfer rate, with great advantages in practical production.

Acknowledgements

The authors gratefully acknowledge the financial support provided by the National Natural Science Foundation of China (Grant No. 51473187) and Science and Technology Project of Guangdong Province (2016A010103013).

References

[1] Nugent P, Belmabkhout Y, Burd SD et al. (2013) Nature 495: 80–84. http://www.nature.com/nature/journal/v495/n7439/abs/nature11893.html#supplementary-information

[2] Francisco-Marquez M, Galano A (2016) J Phys Chem C 120:24476–24481. https://doi.org/10.1021/acs.jpcc.6b08641

[3] Al-Marri MJ, Khader MM, Tawfik M, Qi G, Giannelis EP (2015) Langmuir 31:3569–3576. https://doi.org/10.1021/acs.langmuir.5b00189

[4] Nandi S, De Luna P, Daff TD et al (2015) Sci Adv 1(11):e1500421. https://doi.org/10.1126/sciadv.1500421

[5] Datta SJ, Khumnoon C, Lee ZH et al (2015) Science 350:302–306. https://doi.org/10.1126/science.aab1680

[6] Pham VH, Dickerson JH (2014) ACS Appl Mater Interfaces 6:14181–14188. https://doi.org/10.1021/am503503m

[7] Yang Y, Deng Y, Tong Z, Wang C (2014) J Mater Chem A 2:9994–9999. https://doi.org/10.1039/C4TA00939H

[8] Lastoskie C (2010) Science 330:595–596. https://doi.org/10.1126/science.1198066

[9] Siegelman RL, McDonald TM, Gonzalez MI et al (2017) J Am Chem Soc 139:10526–10538. https://doi.org/10.1021/jacs.7b05858

[10] Boot-Handford ME, Abanades JC, Anthony EJ et al (2014) Energy Environ Sci 7:130–189. https://doi.org/10.1039/C3EE42350F

[11] Yang S, Zhan L, Xu X, Wang Y, Ling L, Feng X (2013) Adv Mater 25:2130–2134. https://doi.org/10.1002/adma.201204427

[12] Chen Z, Deng S, Wei H, Wang B, Huang J, Yu G (2013) Front Environ Sci Eng 7:326–340. https://doi.org/10.1007/s11783-013-0510-7

[13] Zhang W, Liu H, Sun C, Drage TC, Snape CE (2014) Chem Eng Sci 116:306–316. https://doi.org/10.1016/j.ces.2014.05.018

[14] Zhang W, Liu H, Sun Y, Cakstins J, Sun C, Snape CE (2016) Appl Energy 168:394–405. https://doi.org/10.1016/j.apenergy.2016.01.049

[15] Dutcher B, Fan M, Russell AG (2015) ACS Appl Mater Interfaces 7:2137–2148. https://doi.org/10.1021/am507465f

[16] Wang H, Li B, Wu H et al (2015) J Am Chem Soc 137:9963–9970. https://doi.org/10.1021/jacs.5b05644

[17] Ye Y, Xiong S, Wu X et al (2015) Inorganic Chem 55:292–299. https://doi.org/10.1021/acs.inorgchem.5b02316

[18] Evans KA, Kennedy Z, Arey B et al (2018) ACS Appl Mater Interfaces 10:15112–15121. https://doi.org/10.1021/acsami.7b17565

[19] Tan MX, Zhang Y, Ying JY (2013) Chemsuschem 6:1186–1190. https://doi.org/10.1002/cssc.201300107

[20] Wilke A, Weber J (2011) J Mater Chem 21:5226–5229. https://doi.org/10.1039/C1JM10171D

[21] Yang D, Liu P, Zhang N et al (2014) ChemCatChem 6:3434–3439. https://doi.org/10.1002/cctc.201402628

[22] Hu X-M, Chen Q, Zhao Y-C, Laursen BW, Han B-H (2014) J Mater Chem A 2:14201–14208. https://doi.org/10.1039/C4TA02073A

[23] Hug S, Mesch M, Oh H et al (2014) J Mater Chem A 2:5928–5936. https://doi.org/10.1039/c3ta15417c

[24] Zhao Y, Yao KX, Teng B, Zhang T, Han Y (2013) Energy Environ Sci 6:3684–3692. https://doi.org/10.1039/C3EE42548G

[25] Wei J, Zhou D, Sun Z, Deng Y, Xia Y, Zhao D (2013) Nanoscale Res Lett 13:163. https://doi.org/10.1186/s11671-018-2577-3

[26] Tian W, Zhang H, Sun H et al (2016) Adv Funct Mater 26:8651–8661. https://doi.org/10.1002/adfm.201603937

[27] Gomes R, Bhanja P, Bhaumik A (2015) Chem Commun 51:10050–10053. https://doi.org/10.1039/C5CC02147B

[28] Lee JH, Lee HJ, Lim SY, Kim BG, Choi JW (2015) J Am Chem Soc 137:7210–7216. https://doi.org/10.1021/jacs.5b03579

[29] Zhao Y, Liu X, Yao KX, Zhao L, Han Y (2012) Chem Mater 24:4725–4734. https://doi.org/10.1021/cm303072n

[30] Sevilla M, Valle-Vigón P, Fuertes AB (2011) Adv Funct Mater 21:2781–2787. https://doi.org/10.1002/adfm.201100291

[31] Wang J, Senkovska I, Oschatz M et al (2013) J Mater Chem A 1:10951–10961. https://doi.org/10.1039/C3TA11995E

[32] Li P-Z, Zhao Y (2013) Chem Asian J 8:1680–1691. https://doi.org/10.1002/asia.201300121

[33] Kailasam K, Jun Y-S, Katekomol P, Epping JD, Hong WH, Thomas A (2010) Chem Mater 22:428–434. https://doi.org/10.1021/cm9029903

[34] Luo Y, Li B, Liang L, Tan B (2011) Chem Commun 47:7704–7706. https://doi.org/10.1039/C1CC11466B

[35] Hou X, Zhuang L, Ma B, Chen S, He H, Yin F (2018) Chem Eng Sci 181:315–325. https://doi.org/10.1016/j.ces.2018.02.015

[36] He H, Zhuang L, Chen S, Liu H, Li Q (2016) Green Chem 18:5859–5869. https://doi.org/10.1039/C6GC01416J

[37] Mishra PK, Kumar R, Rai PK (2018) Nanoscale 10:7257–7269. https://doi.org/10.1039/C7NR09563E